WARWICK
THE UNIVERSITY OF WARWICK

Manuscript version: Author's Accepted Manuscript
The version presented in WRAP is the author's accepted manuscript and may differ from the published version or Version of Record.

Persistent WRAP URL:
http://wrap.warwick.ac.uk/107324

How to cite:
Please refer to published version for the most recent bibliographic citation information. If a published version is known of, the repository item page linked to above, will contain details on accessing it.

Copyright and reuse:
The Warwick Research Archive Portal (WRAP) makes this work by researchers of the University of Warwick available open access under the following conditions.

Copyright © and all moral rights to the version of the paper presented here belong to the individual author(s) and/or other copyright owners. To the extent reasonable and practicable the material made available in WRAP has been checked for eligibility before being made available.

Copies of full items can be used for personal research or study, educational, or not-for-profit purposes without prior permission or charge. Provided that the authors, title and full bibliographic details are credited, a hyperlink and/or URL is given for the original metadata page and the content is not changed in any way.

Publisher's statement:
Please refer to the repository item page, publisher's statement section, for further information.

For more information, please contact the WRAP Team at: wrap@warwick.ac.uk.

warwick.ac.uk/lib-publications

Electrochemical Reduction of Carbon Dioxide in a Monoethanolamine Capture Medium

Lu Chen,[a] Fengwang Li,[a] Ying Zhang, [a] Cameron L. Bentley,[b] Mike Horne,[c]

Alan M. Bond[a] and Jie Zhang*[a]

[a]School of Chemistry and ARC Centre of Excellence for Electromaterials Science, Monash University, Clayton, Vic 3800, Australia

[b]Department of Chemistry, University of Warwick, Coventry, CV4 7AL, U.K.

[c]CSIRO Minerals Resources Flagship, Clayton, Vic 3168, Australia

Abstract:

A systematic and extensive investigation of the electrocatalytic reduction of carbon dioxide (CO_2) present in a saturated 30% (w/w) monoethanolamine (MEA) aqueous solution has been undertaken at In, Sn, Bi, Pb, Pd, Ag, Cu and Zn metal electrodes. On dissolution of CO_2, the non-conducting monomethanolamine environment is transformed into a conducting electrolyte containing one, as needed to support the electrochemical reduction of CO_2. The species reduced in this widely used CO_2 capture medium is believed to be the free molecular form. Both an increase in the electrode surface porosity and addition of the surfactant cetyltrimethylammonium bromide (CTAB) supress the competing hydrogen evolution reaction, with the latter having a significantly stronger impact. The combination of a porous metal electrode and 0.1% (w/w) of CTAB allows CO_2 to be reduced to CO and formate ($[HCOO]^-$) in the monoethanolomine capture medium, with the product distribution being highly dependent on the identity of the metal electrode used. At an applied potential of -0.8 V vs. the reversible hydrogen electrode (RHE), and using a coralline-like structured In electrode, faradaic efficiencies for the generation of CO and $[HCOO]^-$ are 22.8% and 54.5%, respectively, compared to efficiencies of 2.9% and 60.8% with a porous Pb electrode and 38.2% and 2.4% with a porous Ag electrode. Extensive data for the other 5 electrode surfaces along with characterisation of all 8 metal surfaces by XRD analysis in different formats are also provided. In addition to identifying the optimal conditions for CO_2 reduction, mechanistic details for reaction pathways are proposed in this first electrochemical study in a CO_2 capture medium

1 Introduction:

Since the industrial revolution commenced in the 19th century, fossil fuels have been the major source of energy worldwide.[1] For instance, in the U.S.A., approximately 75% of electricity is produced from the combustion of fossil energy sources.[2] Unfortunately, the combustion of fossil fuels produces environmentally degrading gaseous products, notably carbon dioxide (CO_2), which are accumulating in the earth's atmosphere and contributing to global warming and ocean acidification. Despite significant progress in the utilization of renewable energy such as solar and wind, fossil energy sources will remain significant for some time. Consequently, effective strategies for ameliorating anthropogenic climate change are still urgently needed to reduce CO_2 emissions without adversely affecting existing power plant infrastructure.[3]

Capture of CO_2 through amine scrubbing represents a versatile technique to minimize the impact of its emission. This is a mature technology, which has been widely used in industry for over 70 years.[3] The basic premise of amine scrubbing is that CO_2 gas emitted from coal-fired power plants is initially chemically absorbed into an aqueous amine solution, generating carbamate salts, which are subsequently heated to 100 – 120°C (below the boiling point of the amine) in order to regenerate the amine. The CO_2 gas released from the decomposition of the carbamate is typically compressed to 100 – 150 bar for geological sequestration. The industry standard amine scrubbing formulation is based on 30% (w/w) monoethanolamine (MEA) aqueous solution, which is known to possess a high CO_2 absorption capacity and favourable absorption kinetics.[3-4] During the CO_2 capture process, it is generally accepted that the following chemically reversible reactions occur[5]:

$$CO_2 + MEA \rightleftharpoons MEACOOH \quad (1)$$

$$MEACOOH + MEA \rightleftharpoons [MEAH]^+ + [MEACOO]^- \quad (2)$$

Thus, a CO_2 molecule initially reacts with MEA to form the carbamic acid, MEACOOH (Equation 1), which subsequently reacts with a second MEA molecule to generate the carbamate, $[MEACOO]^-$ (Equation 2). Significantly, the capture medium therefore also provides the electrolyte and conductivity needed for electrochemical reduction

The main barrier to large-scale implementation of CO_2 capture and storage by amine scrubbing is the large amount of energy (and hence cost) associated with amine regeneration (*i.e.*, carbamate decomposition by heating) and subsequent geological sequestration. In a typical amine scrubbing process, a cost of US$50 to $150 per ton of CO_2 has been calculated, with over 90% of the cost associated with the regeneration and compression steps.[3, 6] It follows that developing less energy-intensive, more cost-effective alternatives to amine regeneration and compression for geological sequestration would make the amine scrubbing process more viable for large scale applications. In this work, electrochemical CO_2 reduction has been examined in CO_2 saturated 30% (w/w) MEA aqueous solution in an attempt to provide a viable (particularly when driven by renewable energy) alternative to the existing amine regeneration and CO_2 compression processes.

This paper provides the first report of electrochemical reduction of CO_2 in amine scrubbing media. However, the hydrogen evolution reaction (HER) is invariably found to provide a competing cathodic reaction when CO_2 reduction is carried out in aqueous media and this was expected to also apply in this study. In the CO_2 scrubbing system, protonated amines (*i.e.*, $[MEAH]^+$ in Equation 2) provide the most reactive source of proton.[7] Side-reactions are undesirable in any (electro)catalytic processes, as they lower the faradaic efficiency and product selectivity. An important aspect of (electro)catalyst design for CO_2 reduction was anticipated to be suppression of the HER and hence is considered in detail in this study.

To date, the most widely used (electro)catalysts for CO_2 reduction are based on metals and their metal oxides and complexes.[8] The use of high purity smooth metal foil surfaces have been intensively investigated as cathode catalysts for CO_2 reduction, and it has been shown that the product distribution is highly electrode material dependent.[9] Specifically, the main group metals, indium (In), tin (Sn), bismuth (Bi) and lead (Pb) favour formate ($[HCOO]^-$) generation, while the transition metals, gold (Au), silver (Ag) and zinc (Zn) favour CO generation, while copper (Cu) can also form hydrocarbons. The strong electrode material dependence has mainly been attributed to the differing degrees of surface adsorption of the $CO_2^{-\cdot *}$ radical anion intermediate, which is initially formed during the electro-reduction of CO_2.[9b, 10]

Despite the extensive application, the uses of smooth metal surfaces for CO_2 reduction, suffers disadvantages such as low catalytic activity, limited surface area and low long term stability. Since the surface of an electrocatalyst provides the "active sites" at which the catalytic reaction proceeds (governed by adsorption and/or mass transport of reactants/products), it follows that physical and/or chemical modifications significantly influence catalytic behaviour. For this reason, much effort has been devoted to modifying smooth metal surfaces to enhance CO_2 reduction catalytic activity and supress the HER. Examples of this include nanostructuring, alloying and forming metal oxides. For instance, Hall et al.[11] developed a highly ordered porous Au electrocatalyst, which possessed higher faradaic efficiency for the generation of CO, compared with a smooth (non-porous) surface and Sen et. al.[12] and Dutta et. al.[13] independently developed porous Cu electrodes with dramatically improved catalytic performance for CO_2 reduction relative to the unstructured, smooth surface. These and many other studies highlight the benefit of surface structuring (and roughening) for improving the catalytic properties of metals for CO_2 electro-reduction.

Highly porous metallic catalysts can be prepared by methods such as dealloying[14] (e.g., Ag-Al alloy) and templated metal deposition[15] (e.g., anodic aluminium oxide or gas bubble template). However, electrodeposition with hydrogen gas coevolution (hydrogen bubble templated deposition) is the simplest, cleanest and most efficient technique, allowing the formation of porous morphology without the need of an organic or inorganic template. A wide range of highly ordered porous metallic deposits have been obtained by this method, as summarized in a recent review by Bhargava and co-workers.[15b] This technique relies on the concurrence of the HER and metal deposition reduction processes, and is usually carried out under highly acidic conditions (e.g., 1 M H_2SO_4) to generate a strong and continuous flow of hydrogen (H_2) bubbles. As an alternative to this highly corrosive acid, a medium composed of the protic ionic liquid, dimethylammonium dimethylcarbamate (dimcarb), has been used with the dimethylammonium cation ($[Me_2NH_2]^+$) being the major proton source for the HER.[16] In addition to being less corrosive, dimcarb has two other major advantages over conventional acidic aqueous media: (i) metal salts are typically highly soluble in dimcarb due to strong complexation with Me_2NH and; (ii) during the HER/metal deposition process, electrochemically generated dimethylamine gas from the reduction of $[Me_2NH_2]^+$ is also released, increasing the gas flow rate.

Another approach to inhibit the HER during CO_2 electro-reduction is to introduce surface adsorbates (e.g., surfactants or halides). For example, Jia et al.[17] recently reported that the faradaic efficiency for the generation CO with a smooth Ag electrode can be increased from 50% to 95% by the addition of 20 mM dodecyltrimethylammonium bromide (DTAB) into the reaction medium (0.1 M $NaHCO_3$ solution). The significant enhancement was attributed to the adsorption of the surfactant on metal electrode surface leading to inhibition of the HER while not

interfering with CO evolution. Other, less conventional additives, such as ionic liquids (ILs) are also effective in increasing CO_2 reduction efficiency as shown by Masel et. al.[18] who reported that the addition of 1-ethyl-3-methylimidazolium tetrafluoroborate ($EMIMBF_4$) into aqueous solutions can significantly reduce the overpotential for CO_2 reduction on an Ag electrode and increase the faradaic efficiency for the generation of CO. These authors proposed that the IL lowers the energy of the $CO_2^{-\cdot *}$ radical intermediate, most likely through complexation. A more recent study using *in situ* sum frequency generation spectroscopy showed that a thin layer of $[EMIM]^+$ is adsorbed on the electrode surface under catalytic CO_2 reduction conditions.[19] Furthermore, Rosenthal et al.[20] showed that, ($EMIMBF_4$) can facilitate CO_2 reduction to CO in acetonitrile using the main group metals Sn, Pb, Sb and Bi as the electrocatalysts. Zhao et al.[21] demonstrated that the features highlighted above are not unique to imidazolium cations. In fact, many other organic cations could introduce the same effects.

Based on the information provided above, the possibility of performing CO_2 electro-reduction directly in a CO_2 saturated 30% (w/w) MEA aqueous solution has been investigated using metallic In, Sn, Bi, Pb, Pd, Ag, Cu and Zn electrodes, as representatives of the CO, $[HCOO]^-$ and hydrocarbon formation) classes of CO_2 reduction catalysts, along with assessment of two methods to enhance the (electro)catalytic activity of the metal electrodes, viz,

(i) Addition of a surfactant to the reaction medium

(ii) Introduction of high porosity surface structures

Bulk electrolysis products generated in gas and liquid phases have been characterized by gas chromatography (GC) and ^1H nuclear magnetic resonance (NMR) spectroscopy, respectively.

2 Experimental

2.1 Reagents

The chemicals used and their sources are listed below. In all cases, they were used without further purification. Monoethanolamine (MEA, 99.9%), hydrogen (H_2, standard reference gas), carbon monoxide (CO, standard reference gas), indium chloride ($InCl_3$, 98%), tin sulfate ($SnSO_4$, >95%), bismuth nitrate ($Bi(NO_3)_2$, 98%), lead acetate ($Pb(Ac)_2$, 99.999%), zinc acetate ($Zn(Ac)_2$, 99.99%), copper(I) chloride (CuCl, 99.99%), silver nitrate ($AgNO_3$, 99%), palladium nitrate ($Pd(NO_3)_2$, 95.0%), zinc (Zn, 99.99%), palladium (Pd, 99.95%), dimethyl sulfoxide (DMSO, 99.9%), deuterium oxide (D_2O, 99.9%), cetyltrimethylammonium bromide (CTAB, 98%), sodium dodecyl sulfate (SDS, 98%), 4-octylphenol polyethoxylate (Triton X-100, 98%) and cobaltocenium hexafluorophosphate ($[Cc]^+[PF_6]^-$, 98%) were all from Sigma-Aldrich. Nitrogen (N_2, 99.999%), helium (He, 99.9%) and carbon dioxide (CO_2, 99.9%) were from Air Liquide, Australia. Indium (In), tin (Sn), bismuth (Bi), lead (Pb), silver (Ag) were purchased from Zr-industrial, Shanghai, China, each with a purity of 99.9%. Copper (Cu) was purchased from Good Fellow, with a purity of 99.99%. Dimethylammonium dimethylcarbamate was synthesized by literature procedures. [22]

2.2 Electrochemical instrumentations and procedures

All cyclic voltammetric and (potentiostatic) bulk electrolysis experiments were carried out at room temperature (22 ± 2°C) in the three electrode format using a CHI760D electrochemical workstation (CHI Instruments, Austin, Texas, USA). Smooth or porous metal, a platinum plate and Ag/AgCl (3M NaCl) were used as the working (cathode), counter (anode) and reference electrode, respectively.

The porous metallic electrodes were fabricated by the hydrogen bubble templated metal deposition technique in dimcarb by holding the potential at very negative values (e.g. -4.0 V vs. $Cc^{0/+}$). Unless otherwise stated, all porous metal surfaces were deposited with their own metal substrates (i.e. Pb deposited on Pb, Sn on Sn and Bi on Bi). This allows the influence of the substrate to be omitted. In the porous metal electrodeposition process, a graphite rod was used as the counter electrode (anode) and the quasi-reference electrode consisted of a small, fritted glass tube containing a silver wire in contact with neat dimcarb. The quasi reference electrode potential was very stable and calibrated against the $Cc^{0/+}$ process, post electrolysis. Full details of the deposition process are provided in the Supporting Information.

The 30% (w/w) MEA aqueous solution was saturated with CO_2 by continuous bubbling with this gas for 30 minutes. The stoichiometric ratio of MEA to CO_2 is 2:1 in the saturated solution (see Equations 1 and 2), and the total concentration of CO_2 is approximately 2.46 M. It should be noted that although the CO_2 absorption process is exothermic, the temperature of the solution returns to room temperature, after approximately 30 minutes. In addition, since the saturated 30% (w/w) MEA aqueous solution is relatively corrosive, after each measurement, all the electrodes were immediately removed from the solution. Bulk electrolysis was conducted in a gas-tight two-compartment H-shape electrolysis cell under a CO_2 rich atmosphere, with a porous glass frit separating the anodic and cathodic half-cells. High purity CO_2 gas was introduced to remove oxygen prior to electrochemical measurements and the CO_2 saturated electrolysis cell was sealed tightly with a rubber stopper. The pH of the neat 30% (w/w) MEA aqueous solution is 12.3 and after bubbling CO_2 for 30 minutes, drops to 8.55. All potentials were initially measured versus an Ag/AgCl (3M NaCl) reference

electrode and then converted to the reversible hydrogen electrode (RHE) scale using the relationship: E vs. (RHE) = E vs. (Ag/AgCl) + 0.059pH + 0.209 V (at 22°C).

2.3 Characterization techniques.

The surfaces of the electrodes were imaged using a Magellan 400 FEGSEM scanning electron microscope (SEM). Powder X-ray Diffraction (PXRD) data were collected with a Bruker D2 X-ray powder diffractometer (Cu Kα1 radiation) using a scan rate of 0.5 degree per minute. An Agilent (7820 A) Gas Chromatography (GC) system, equipped with a HP-plot molesieve (5Å) column and a thermal conductivity detector (TCD) was used to identify gaseous products generated in the headspace of the bulk electrolysis cell. In order to achieve adequate peak separation, a shorter column with He carrier gas was used to detect CO and a longer column with a N_2 carrier gas to detect H_2. Calibration curves for H_2 and CO were constructed by injecting of a known amount of pure H_2 and CO and plotting the peak area against the amount injected. Further details on the analysis procedures are reported elsewhere.[22] In some cases, the total calculated faradaic efficiency deviates slightly from the theoretical limit of 100% (typically by ± 5%), which is attributable to experimental uncertainties, as addressed previously.[22-23] Finally, CO_2 bubbling times of 30 minutes were used rather than a few minutes which is typical in the operation of post-combustion capture (PCC) pilot plants. The longer times were necessary to provide accurate and reproducible results.

3 Results and Discussion

Neat 30% MEA (w/w) aqueous solution is composed predominantly of the molecular species, H_2O and MEA, and is therefore a poor ionic conductor. For this reason, conventional voltammetric and polarization measurements cannot be carried out in this medium without the addition of supporting electrolyte. This meant that the catalytic activity of the metal electrodes towards CO_2 reduction could not be evaluated by comparison of the voltammetric response in the presence and absence of CO_2, as is typically done in aqueous bicarbonate media. Direct measurement (quantification) of the products formed during bulk electrolysis was therefore required under saturated CO_2 conditions, as outlined in the Experimental Section. This approach was successful because after saturation with CO_2, 30% (w/w) MEA aqueous solution now contains around 2.5 M concentrations of the ionic species $[MEAH]^+$ and $[MEACOO]^-$ (see Equations 1 and 2). This achieves high ionic conductivity, and avoids the need to add external supporting electrolyte.

Bulk electrolysis was performed potentiostatically, usually at applied potentials of -0.8, -1.1 and -1.3 V vs. RHE, allowing the influence of the applied potential on the distribution of products to be investigated. In the case of Pd however, the HER is kinetically facile, necessitating the use of less negative potentials of -0.1, -0.4 and -0.8 V vs. RHE. It should be noted that the current density at a given applied potential varies from metal-to-metal, reflecting the fact that CO_2 reduction overpotential (and hence CO_2 reduction kinetics) is material dependent.

3.1 Bulk electrolysis on smooth metal surfaces

The 8 smooth metal surfaces (In, Sn, Bi, Pb, Pd, Ag, Cu and Zn) investigated as electrocatalysts for CO_2 reduction in 30% (w/w) MEA aqueous solution (*i.e.*, PCC

media) were selected on the basis that they all are effective catalysts for CO_2 reduction in aqueous $[HCO_3]^-$ solution.[9] The bulk electrolysis product distribution for each metal as a function of applied potential are summarized in Table 1.

Table 1: Bulk electrolysis product distributions[a] (faradaic efficiencies for the generation of H_2, CO and $[HCOO]^-$) measured at 8 smooth metal electrodes at three designated applied potentials in CO_2 saturated 30% (w/w) MEA aqueous solution.

	Potential	Faradaic Efficiency			
		H_2	CO	$[HCOO]^-$	sum
In	-0.8	85.2%	4.8%	2.4%	92.4%
	-1.1	95.7%	1.5%	0.1%	97.2%
	-1.3	98.9%	0.7%	0.1%	99.7%
Sn	-0.8	84.9%	5.7%	5.2%	95.8%
	-1.1	95.7%	1.3%	1.0%	98.0%
	-1.3	97.4%	0.7%	1.0%	99.1%
Bi	-0.8	60.8%	4.1%	**35.7%**	100.6%
	-1.1	82.9%	2.1%	**10.1%**	95.1%
	-1.3	88.8%	1.1%	**5.3%**	95.2%
Pb	-0.8	97.0%	0.1%	3.7%	100.8%
	-1.1	97.8%	0.1%	0.3%	98.2%
	-1.3	101.7%	0.1%	1.6%	103.4%
Pd	-0.1	87.8%	b	1.0%	88.8%[c]
	-0.4	81.6%	b	1.0%	82.6%[c]
	-0.8	80.0%	b	0.7%	80.7%[c]
Ag	-0.8	85.8%	**12.4%**	1.3%	99.5%
	-1.1	93.0%	**6.1%**	1.0%	100.1%
	-1.3	94.2%	**2.3%**	1.2%	97.7%
Cu	-0.8	90.2%	0.5%	0.8%	91.5%
	-1.1	93.4%	b	0.6%	94.0%
	-1.3	94.2%	b	0.7%	94.9%
Zn	-0.8	97.3%	0.8%	2.1%	100.2%
	-1.1	104.7%	0.5%	0.8%	106.0%
	-1.3	95.7%	0.3%	0.2%	96.2%

a: The results obtained from the best performing catalysts are highlighted in **bold**.
b: Below the detection limit
c: Underestimated due to hydride formation

As can be seen from Table 1, the majority of the bulk smooth metal surfaces exhibit little catalytic activity towards CO_2 reduction in the PCC medium, with H_2 being the

predominant product, although notably, Bi is able to reduce CO_2 to $[HCOO]^-$ with faradaic efficiencies of 35.7%, 10.1% and 5.3% at potentials of -0.8, -1.1 and -1.3 V vs. (RHE), respectively. It should also be noted that a spontaneous (galvanic) reaction was also observed when the Zn electrode was left in the solution for approximately 1 hour in the absence of external potential bias, as is demonstrated in Figure S1. Additionally, the Ag electrode was able reduce CO_2 to CO, with faradaic efficiencies of 12.4%, 6.1% and 2.3% at potentials of -0.8, -1.1 and -1.3 V vs. (RHE), respectively. The potential-dependent behaviour is generally attributed to the change in the competition between the HER and CO_2 reduction, with the more negative potential favouring the HER reaction due to mass-transport limitations associated with CO_2 reduction. [10, 24]

Generally, the low faradaic efficiency associated with use of the smooth metal surfaces excludes their use as electrocatalysts for CO_2 reduction. Clearly, as highlighted in the Introduction Section, in order to enhance the catalytic performance, the HER needs to be supressed on these metallic surfaces, as is explored below.

3.2 Bulk electrolysis on smooth metal surfaces in the presence of surfactant

The cationic, anionic and non-ionic surfactants, CTAB, SDS and Triton X-100, respectively, were initially screened at a concentration of 0.1% (w/w) for their ability to supress the HER during CO_2 reduction at a smooth In electrode in 30% (w/w) MEA aqueous solution. Analysis of the bulk electrolysis products obtained at a controlled potential of -0.8 V vs. (RHE) reveals a strong dependence on the type of surfactant employed, as summarized in Figure 1(a). In the presence of the cationic surfactant CTAB, the faradaic efficiencies for the generation of CO and $[HCOO]^-$ increase significantly from 4.8% and 2.4% to 17.0% and 45.4%, respectively, dramatically improving the catalytic performance of the In electrode. By contrast, the anionic

surfactant, SDS, supressed the CO_2 to CO reduction pathway (faradaic efficiency dropped from 4.8% to 0.6%) but enhanced the CO_2 to $[HCOO]^-$ pathway (faradaic efficiency increased from 2.4% to 14.7%). Finally, Triton X-100 did not significantly influence CO_2 reduction, as the faradaic efficiencies for the generation of CO and $[HCOO]^-$ are 1.9% and 0.5% respectively, very similar to those obtained in the absence of this surfactant. Clearly, the cationic surfactant, CTAB, is very effective in promoting the catalytic properties of In towards CO_2 reduction in 30% (w/w) MEA aqueous solution, while SDS (anionic) and Triton X 100 (non-ionic) are not effective.

The voltammograms (Figure S2) obtained in the presence and absence of 0.1% (w/w) of the surfactant show that the current density decreases by ~40% by addition of 0.1% (w/w) CTAB, while current density remains relatively unaffected by the presence of the other surfactants. These results are consistent with the bulk electrolysis data, which suggest that CTAB supresses the HER and enhances the kinetics of the CO_2 reduction process, presumably through the provision of nitrogen binding sites for CO_2/ $CO_2^{-\cdot *}$ adsorption. Results obtained by Zhao et al.[21] also showed that surface adsorbed nitrogen containing organic cations could effectively supress the HER and promote CO_2 reduction reactions in acetonitrile containing 2.0 % (w/w) H_2O, as do the findings of Jia et al.[17] in aqueous $[HCO_3]^-$ media.

The concentration/mass ratio of CTAB was optimized by performing bulk electrolysis, again at -0.8 V vs. (RHE), on a smooth In electrode in the presence of 0.01, 0.1 and 1% surfactant. Analysis of the electrolysis products (Figure 1b) clearly reveals that there is a critical mass ratio of CTAB (approx. 0.1% w/w) required to achieve optimum CO_2 reduction performance, with no further improvement achieved by adding more surfactant. Interestingly, adding 0.01% (w/w) CTAB, only enhances the CO_2 to $[HCOO]^-$ pathway (faradaic efficiency improves from 2.4% to 34.9%), whereas 0.1%

(and above) enhances both the CO_2 to $[HCOO]^-$ generation (faradaic efficiency improved from 2.4% to 45.4%) and CO_2 to CO generation (faradaic efficiency improved from 4.8% to 17.0%) pathways. An identical set of surfactant concentration optimization experiments carried out with a smooth Sn electrode also lead to the conclusion that 0.1% (w/w) CTAB gives optimal performance (*e.g.*, see Figure S3). On the basis of In and Sn data, all 8 metals (see Table 2) were re-screened for CO_2 reduction performance at 3 potentials in the presence of 0.1% (w/w) CTAB; the bulk electrolysis reduction product distributions are summarized in Table 2.

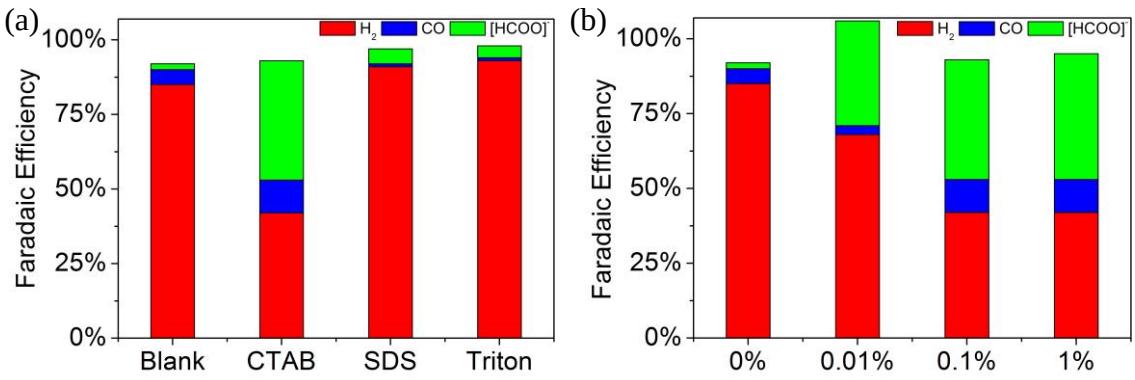

Figure 1: (a) Faradaic efficiencies of the electrolysis products obtained with a smooth In electrode at a potential of -0.8 V vs. (RHE) in CO_2 saturated 30% (w/w) MEA aqueous solution with 0.1% (w/w) of CTAB, SDS or Triton X-100. (b) Faradaic efficiencies of the electrolysis products obtained with a smooth In electrode at a potential of -0.8 V vs. (RHE) in CO_2 saturated 30% (w/w) MEA aqueous solution with 0%, 0.01%, 0.1% or 1% (w/w) CTAB.

Table 2: Bulk electrolysis product distributions[a] (faradaic efficiencies for the generation of H_2, CO and $[HCOO]^-$) measured at 8 smooth metal electrodes using three designated applied potentials in CO_2 saturated 30% (w/w) MEA aqueous solution containing 0.1% (w/w) CTAB.

	Potential	Faradaic Efficiency			
		H_2	CO	$[HCOO]^-$	sum
In	-0.8	41.9%	**17.0%**	**45.4%**	104.3%
	-1.1	42.0%	**10.7%**	**39.4%**	92.1%
	-1.3	44.3%	**11.2%**	**36.5%**	92.0%
Sn	-0.8	68.6%	9.0%	**19.0%**	96.6%
	-1.1	78.5%	3.6%	**16.4%**	98.5%
	-1.3	93.4%	2.6%	**2.0%**	98.0%
Bi	-0.8	69.5%	7.0%	24.3%	100.8%
	-1.1	87.1%	4.9%	7.1%	99.1%
	-1.3	93.4%	2.6%	3.9%	99.9%
Pb	-0.8	79.6%	1.9%	8.5%	90.0%
	-1.1	79.2%	3.0%	8.7%	90.9%
	-1.3	85.1%	3.5%	6.1%	94.7%
Pd	-0.1	91.6%	b	4.0%	95.6%
	-0.4	87.3%	b	4.1%	91.4%
	-0.8	96.0%	b	0.1%	96.1%
Ag	-0.8	62.8%	**33.4%**	2.0%	100.8%
	-1.1	84.7%	**15.9%**	2.8%	103.4%
	-1.3	89.5%	**9.2%**	1.7%	100.4%
Cu	-0.8	79.7%	1.7%	19.1%	100.5%
	-1.1	98.1%	b	0.5%	98.6%
	-1.3	91.0%	b	0.1%	91.1%
Zn	-0.8	103.0%	3.7%	5.4%	112.1%
	-1.1	91.4%	2.9%	2.0%	96.3%
	-1.3	102.0%	0.5%	2.0%	104.5%

a: The catalysts showing the greatest enhancement in CO_2 reduction performance (*i.e.*, CO or $[HCOO]^-$ formation) are highlighted in **bold**.
b: Below the detection limit

By comparing the data in Tables 1 and 2, it is clear that CTAB enhances CO_2 reduction catalytic performance in saturated 30% (w/w) MEA aqueous solution, irrespective of the metal surface. Of the 8 metals investigated, In and Ag showed the greatest enhancements in terms of the generation of CO and $[HCOO]^-$. In the case of In, faradaic efficiencies for the generation of CO and $[HCOO]^-$ are 17.0% and 45.4% at a potential of -0.8 V vs. (RHE), and do not change significantly over the potential range of –0.8 V to –1.3 V vs. (RHE). For Ag, the faradaic efficiencies for the generation of CO and

$[HCOO]^-$ are 33.4% and 2.0% at an applied potential of –0.8 V vs. (RHE). However, there is a clear potential dependence of the product distribution in the case of Ag (and most of the other metals), as CO_2 reduction performance clearly degrades at more negative potentials (*e.g.*, -1.1 and -1.3 V in Table 2). Finally, it is worth noting that the molar ratio of the gaseous products, H_2 and CO, at –0.8 V vs. (RHE) is approximately 2:1, meaning it could be utilized directly as syngas in industrial applications.

In principle, if CTAB was acting as a homogeneous catalyst mediating the CO_2 reduction process, then the identity of the metal substrate would not be expected to influence the product distribution. Clearly, this is not the case (see Table 2), as, for example, Ag favours the formation of CO, while Bi prefers to generate $[HCOO]^-$ and In generates both CO and $[HCOO]^-$. This implies catalytic participation of the metal surface in adsorption/desorption of the reactant/product in the CO_2 reduction process.

3.3 Bulk electrolysis on porous (structured) metal surface

In order to probe the influence of surface structuring on catalytic performance in CO_2 saturated 30% (w/w) MEA aqueous medium, porous electrodes were prepared from the 8 metals of interest in this study (see Tables 1 and 2) by hydrogen bubble evolution templated electrodeposition. The general premise is that the generation of H_2 gas bubbles occurs simultaneously with the metal deposition process, and as a result, the growth of the metal follows the edge of the bubbles. For this reason, changes in the relative rate of bubble generation and metal deposition achieved through changing the applied potential or deposition substrate will change the morphology of the deposit. In this study, electrodeposition was carried out in the distillable protic ionic liquid, dimcarb, meaning the co-generated gases were H_2 and Me_2NH from the HER involving $[Me_2NH_2]^+$. The surface structures can be generally categorized into three groups based on morphology: (i) porous structure (Sn, Bi, Pb, Cu, Ag and Pd); (ii) coralline-like

structure (In); and (iii) two-dimensional layered structure (Zn). The morphology of the porous structured materials is very similar with what is obtained from deposition in strongly acidic solutions (e.g., 1 M H_2SO_4). It needs to be noted that a significant effort applied into attempting to deposit porous In and Zn through changing the substrate material, type of metal salts, concentration, deposition parameters and introducing additives was not successful. Electrodepositing porous In and Zn in dimcarb seems to be very challenging.

The influence of the applied potential on the morphology of the porous deposit (i.e., pore size) was also studied, using Cu as the model element. As can be seen from Figure S5, on increasing the applied potential, the pore size tends to increase as noted for Cu deposits obtained from strong acidic solution (e.g. 1 M H_2SO_4).[15b, 25] Similar observations were also made with Pb, Sn, Bi and Pd.

In order to identify the crystallographic structure of the porous deposits, powder XRD was used on samples prepared on a graphite plate using the deposition parameters given above (it is assumed that the substrate does not influence the crystallographic structure of the deposits which is typically 500 μm thick). As shown in Figure S6, all metallic deposits are polycrystalline, with no strongly preferred crystallographic orientation. In addition, they are all well-crystallized, with crystallite sizes of over 50 nm based on use of the Scherrer Equation.[26] No peaks attributable to metal hydrides were observed, despite the fact that the deposits are surrounded by H_2 gas during the electrodeposition process. Perhaps surprisingly, no evidence for PdH_x was evident from the XRD data. Small peaks attributable to metal oxides in the XRD spectra, are likely to have been introduced by reaction with oxygen during the sample transfer process required for powder XRD characterization.

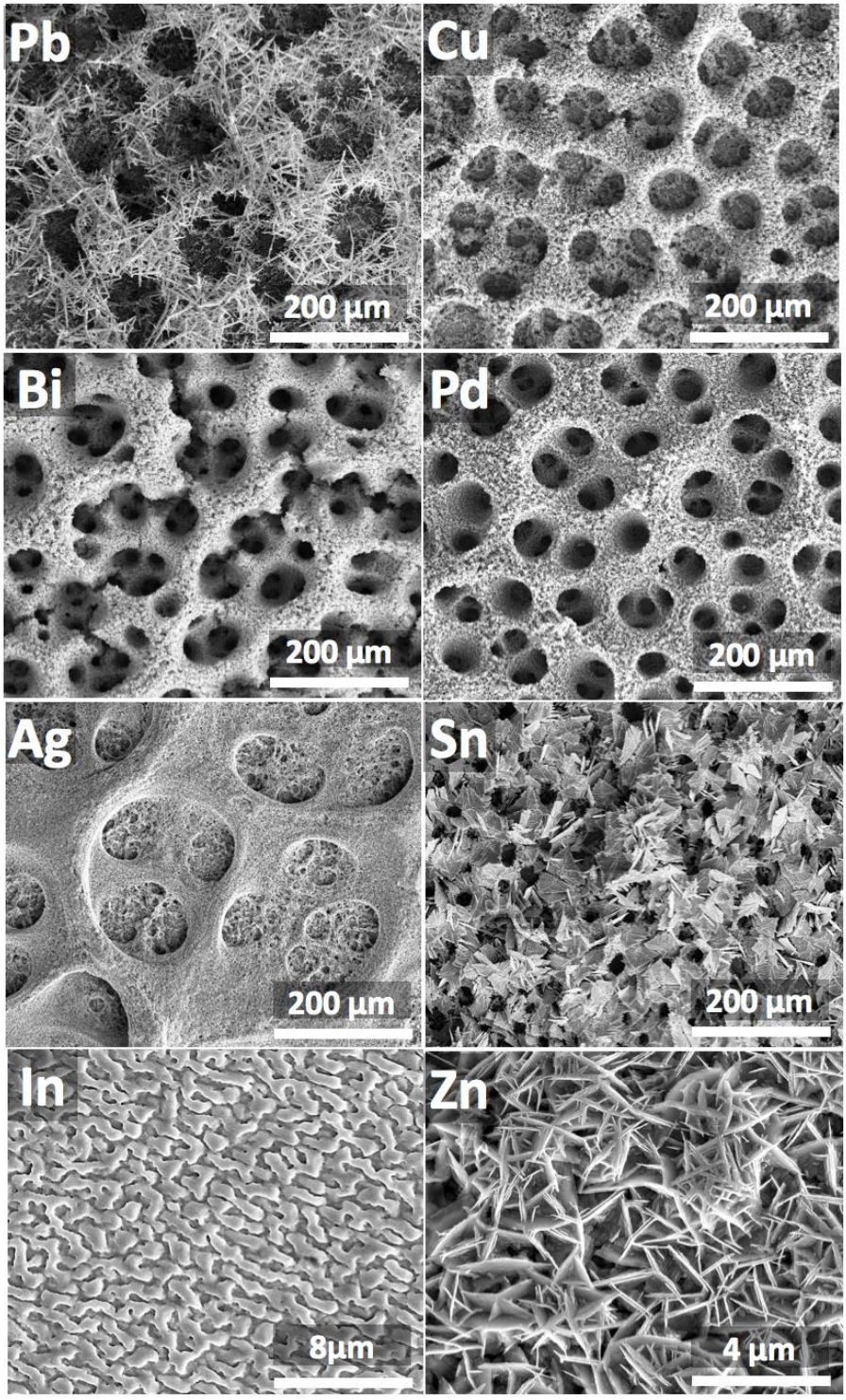

Figure 2: SEM images of the metallic deposits (metals and scale bars indicated on the respective images) formed by hydrogen bubble templated metal deposition. Images obtained at higher magnifications and the deposition parameters are provided in the Supporting Information, Figure S4 and Table S1, respectively.

After deposition, the porous/structured metallic deposits were used as electrocatalysts for CO_2 reduction in CO_2 saturated 30% (w/w) MEA aqueous solution; the bulk electrolysis product distributions are contained in Table 3. By comparing the data in Tables 1 and 3, it is clear that the structured metal surfaces are more effective as CO_2 reduction catalysts than smooth ones, as most porous metals generate significantly more CO and $[HCOO]^-$ (relative to H_2). However, a comparison of data in Tables 2 and 3 indicates that surface structuring is less effective than the addition of 0.1% (w/w) CTAB, with only Ag showing a comparable enhancement in catalytic activity, with a faradaic efficiency for the generation of CO of 39.1% at -0.8 V vs. (RHE). Again, faradaic efficiencies for the generation of CO and $[HCOO]^-$ diminish significantly upon applying more negative potentials to porous electrodes (see explanation given above).

A significant enhancement in catalytic activity of Ag upon surface structuring has previously been reported.[27] The reason proposed is related to the relative availabilities of protons and CO_2 within the pores. In CO_2 saturated 30% (w/w) MEA aqueous medium, the (bulk) pH is about 8.55, meaning that free proton concentration is very low relative to that of CO_2, as discussed in more detail below. Due to mass-transport limitations within the porous structure, rapid consumption of protons in the pores will lead to an increase in the local pH, thereby suppressing the HER. Even though, depletion of CO_2 within the pores also is expected, this has less impact, due to the initially much higher concentration of CO_2 compared to protons. The effectiveness of the porous structuring on improving CO_2 reduction efficiency is dependent on the identity of the metals (Tables 1 and 3). This is unsurprising since the hindrance to mass-transport is highly dependent on the identities of the metals due to the differences in their porosity (see Figure 2).

Table 3: Bulk electrolysis product distributions[a] (faradaic efficiencies for the generation of H_2, CO and $[HCOO]^-$) are determined using 8 porous/structured metal electrodes at three designated applied potentials in CO_2 saturated 30% (w/w) MEA aqueous solution.

	Potential	Faradaic Efficiency			
		H_2	CO	$[HCOO]^-$	sum
In	-0.8	82.3%	2.0%	13.4%	97.7%
	-1.1	91.4%	0.5%	6.6%	98.5%
	-1.3	95.6%	0.1%	5.3%	101.0%
Sn	-0.8	79.2%	8.9%	4.1%	92.2%
	-1.1	86.7%	6.3%	2.4%	95.4%
	-1.3	95.6%	2.0%	3.3%	100.9%
Bi	-0.8	67.5%	5.2%	**18.3%**	91.0%
	-1.1	85.7%	2.4%	**8.2%**	96.3%
	-1.3	84.6%	1.9%	**7.7%**	94.2%
Pb	-0.8	92.5%	0.9%	2.2%	95.6%
	-1.1	101.8%	0.4%	4.5%	106.7%
	-1.3	95.0%	0.6%	4.2%	99.8%
Pd	-0.5	75.9%	0.1%	2.5%	83.0%
	-0.8	85.9%	0.1%	4.1%	90.0%
Ag	-0.8	60.2%	**39.1%**	0.2%	99.5%
	-1.1	85.5%	**12.0%**	3.9%	101.4%
	-1.3	91.0%	**5.0%**	2.1%	98.1%
Cu	-0.8	96.0%	0.1%	0.1%	96.2%
	-1.1	98.5%	0.1%	1.7%	100.3%
	-1.3	101.9%	b	0.7%	102.6%
Zn	-0.8	113.8%	0.6%	9.0%	123.4%
	-1.1	120.0%	0.2%	2.4%	122.6%
	-1.3	118.5%	0.4%	2.2%	121.1%

a: The results obtained from the best performing catalysts are highlighted in **bold**.
b: below the detection limit

3.4 Bulk electrolysis on porous (structured) metal surfaces in the presence of surfactant

In the final set of experiments, the structured metal electrodes, which are generally more efficient CO_2 reduction catalysts than the smooth surfaced ones (e.g., see Tables 1 and 3), were employed as electrocatalysts for the reduction of CO_2 in saturated 30% (w/w) MEA aqueous solution in the presence of 0.1% (w/w) CTAB, which also promotes the formation of CO_2 reduction products (e.g. see Tables 1 and 2). This

combination of structured electrodes and HER-suppressing surfactant was concluded to achieve optimum catalytic performance, as evidenced by data summarized in Table 4. In the presence of CTAB, the catalytic performance of structured In and Ag drastically improves, with CO and $[HCOO]^-$ making up more than 40% of the total reduction products at an applied potential of -0.8 V vs. (RHE). Notably porous Pb, which was previously a poor electrocatalyst (*e.g.*, see Table 3) in now an exceptional one for the production of $[HCOO]^-$ in the presence of CTAB, with a faradaic efficiency of 60.8% at −0.8 V vs. (RHE). Clearly for metals such as Pb, surface structuring and the addition of CTAB provide a synergistic effect for catalytic CO_2 reduction.

Table 4: Bulk electrolysis product distributions[a] (faradaic efficiencies for the generation of H_2, CO and $[HCOO]^-$) measured at 8 porous/structured metal electrodes at three designated applied potentials in CO_2 saturated 30% (w/w) MEA aqueous solution containing 0.1% (w/w) of CTAB.

	Potential	Faradaic Efficiency			
		H_2	CO	$[HCOO]^-$	sum
In	-0.8	14.3%	**22.8%**	**54.5%**	91.6%
	-1.1	53.3%	**7.6%**	**30.0%**	90.9%
	-1.3	74.2%	**3.9%**	**19.6%**	97.7%
Sn	-0.8	66.1%	16.6%	11.6%	94.3%
	-1.1	81.7%	9.0%	4.8%	95.5%
	-1.3	90.2%	5.0%	4.4%	99.6%
Bi	-0.8	58.5%	4.9%	36.0%	99.4%
	-1.1	79.5%	3.4%	13.0%	95.9%
	-1.3	86.3%	0.5%	5.3%	92.1%
Pb	-0.8	36.7%	2.9%	**60.8%**	100.4%
	-1.1	66.4%	3.1%	**21.5%**	91.0%
	-1.3	79.7%	2.8%	**14.7%**	97.2%
Pd	-0.5	69.4%	0.2%	1.0%	71.0%
	-0.8	75.3%	a	1.1%	76.0%
Ag	-0.8	56.0%	**38.2%**	2.4%	96.6%
	-1.1	62.8%	**34.3%**	1.6%	98.7%
	-1.3	79.7%	**20.0%**	1.3%	101.0%
Cu	-0.8	98.6%	0.1%	1.1%	99.8%
	-1.1	103.0%	0.1%	0.8%	103.9%
	-1.3	98.0%	a	0.8%	98.8%
Zn	-0.8	99.2%	1.4%	7.3%	107.9%
	-1.1	115.3%	2.4%	3.3%	121.0%
	-1.3	110.8%	1.9%	3.1%	115.8%

a: The results obtained from the best performing catalysts are highlighted in **bold**.
b: below the detection limit

3.5 Summary and further mechanistic considerations

The role of surfactant and the surface structure of the metal have been discussed above. Other aspects of electrocatalysis, such as the nature of the reactive substrate and the source of protons participating in the proton coupled electro-reduction of CO_2 or the undesirable HER, are the foci of this Section.

As alluded to in the Introduction Section, the predominant species in 30% (w/w) MEA aqueous solution change as CO_2 is dissolved (see Equations 1 and 2), with the amount of MEA decreasing and $[MEAH]^+$ and $[MEACOO]^-$ increasing correspondingly, until

the molecular ratio limit of CO_2/MEA = 0.6 is reached. [5a, 5d, 5g] The ^{1}H NMR spectra of 30% (w/w) MEA aqueous solution with a CO_2/MEA molar loadings of 0.48 and 0.6 is consistent with reported data, confirming the high dependence of species on CO_2 loading (Figure S7). The main CO_2 containing species present in the solution are expected to be $[MEACOO]^-$ (major species) and free CO_2 molecules (minor species). [28] In order to identify which molecule is the electroactive (i.e., reactive) species, control experiments were performed in 30% (w/w) MEA aqueous solution without free molecular CO_2 (i.e., the CO_2/MEA molar loading is below 0.6), while $[MEACOO]^-$ is still present.[5f] The bulk electrolysis experiments were carried out in 30% (w/w) MEA aqueous solution with three different CO_2 loadings (0.3, 0.4 and 0.48) using smooth In and Ag electrodes in the presence of 0.1% (w/w) of CTAB. As can be seen from Figure 3, H_2 dominates the electrolysis product when using In or Ag, irrespective of the applied potential (Table S2). This is a strong indicator that free CO_2 is the active species which takes part in catalytic electro-reduction process. This result is consistent with the finding described in Section **3.1** which indicates a mass-transport limitation associated with CO_2 reduction. No mass transport limitation is expected if the abundant $[MEACOO]^-$ is the source of CO_2.

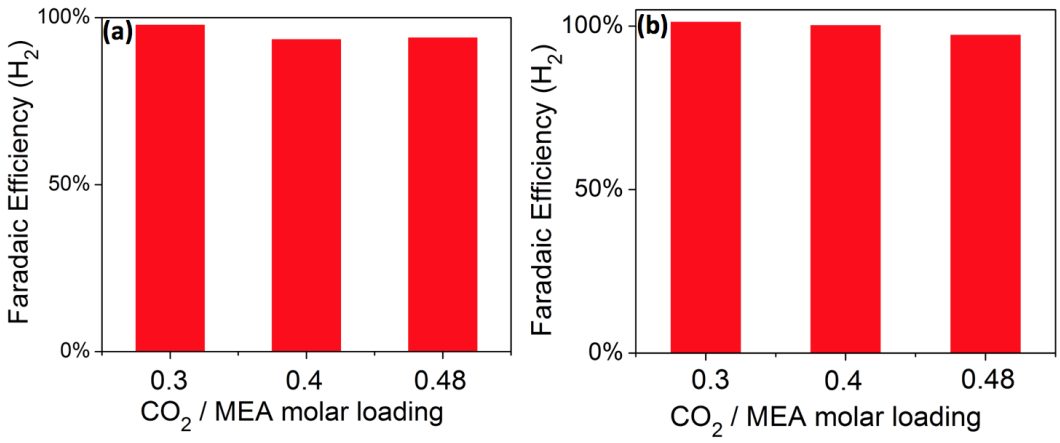

Figure 3: Faradaic efficiencies for generating H_2 obtained with smooth (a) indium (b) silver electrodes in 30% (w/w) MEA aqueous solution with three designed CO_2 loadings (0.3, 0.4 and 0.48), in the presence of 0.1% (w/w) CTAB.

Since CO_2 reduction involves a proton-coupled electron transfer process, it is important to identify the proton source. In bulk water, it is well known that CO_2 reversibly forms carbonic acid, H_2CO_3, a weak acid that partially dissociates to form H^+ and $[HCO_3]^-$. As shown in Equation (3).

$$CO_2 + H_2O \rightleftharpoons H_2CO_3 \rightleftharpoons H^+ + [HCO_3]^- \qquad (3)$$

where H^+ is a 'solvated proton' (e.g., $[H_3O]^+$ in H_2O). The hydration equilibrium and acid dissociation constants of H_2CO_3 are 2.6×10^{-3} and 4.5×10^{-7} at 25°C, respectively.[29] Of the species participating in the reaction described in Equation 3, $[HCO_3]^-$ is predominant in CO_2 saturated 30% (w/w) MEA aqueous solution (pH ≥ 8.55). With this in mind, and considering that the pK_a values of $[MEAH]^+$, $[HCO_3]^-$ and H_2O in bulk water are 9.4, 10.3 and 15.7,[30] respectively, we propose that the protons consumed in the CO_2 reduction mechanism(s) shown below are from $[MEAH]^+$ and not from H_2O, H_2CO_3 or $[HCO_3]^-$. Consequently, the HER is proposed to occur through the pathway shown in Equation (4).

$$2[MEAH]^+ + 2e^- \rightleftharpoons 2MEA + H_2 \qquad (4)$$

Since free CO_2 is the active substrate, the following mechanism for the generation of $[HCOO]^-$ is proposed, which is analogous to the one previously described in aqueous solution.[9a, 31] Firstly, CO_2 is reduced to $CO_2^{-\cdot *}$ radical anion (superscript "*" is used to indicate a surface adsorbed species) via a one electron transfer process, as shown in Equation 5. The $CO_2^{-\cdot *}$ radical anion then desorbs from the electrode surface and takes a proton from $[MEAH]^+$ to generate the $HCOO^{\cdot *}$ radical, which is subsequently reduced in a one-electron transfer process, generating $[HCOO]^-$, as shown in Equation 6,

$$CO_2 + e^- \rightleftarrows CO_2^{-\cdot *} \quad (5)$$

$$CO_2^{-\cdot *} + [MEAH]^+ + e^- \rightleftarrows [HCOO]^- + MEA \quad (6)$$

where * stands for the adsorption vacancy sites on the metal surface. Since there is an abundance of available protons of $[MEAH]^+$, the possibility of oxalate formation through dimerization of the $CO_2^{-\cdot *}$ radical anion which occurs in aprotic media [32] is very limited, as is the case in other protic media.[9b]

With respect to the formation of CO, mechanisms analogous to that in conventional media, which involves free CO_2 as the reactant, are proposed.[9a, 33] In the first pathway, a $CO_2^{-\cdot *}$ radical formed via the reaction described in Equation 5 combines with a proton from $[MEAH]^+$ on the electrode surface and receives an electron to generate CO, as shown in Equation 7.

$$CO_2^{-\cdot *} + 2[MEAH]^+ + e^- \rightarrow CO + 2MEA + H_2O \quad (7)$$

Although, CO could also form in a different pathway: two desorbed $CO_2^{-\cdot *}$ radicals combine to form CO and carbonate $[CO_3]^{2-}$ through an overall reaction described in Equation 8, the pathway described in Equation 7 is considered more favourable due to the abundance of $[MEAH]^+$ present in the solution.

$$CO_2^{-\cdot *} + CO_2^{-\cdot *} \rightarrow CO + [CO_3]^{2-} \quad (8)$$

4 Conclusions

In this first report of electrochemical CO_2 reduction in the industrial CO_2 capture medium, 30% (w/w) MEA aqueous solution, two methods have been introduced to improve the otherwise poor faradaic efficiencies for the generation of CO and $[HCOO]^-$ achieved with flat metal surfaces, (i) increasing the surface porosity of the metallic electrode surface and (ii) adding a surfactant into the reaction media. The cationic surfactant CTAB, at an optimised concentration of 0.1% (w/w), effectively supresses the competitive HER. It is assumed that this desirable outcome is achieved because the adsorption of CTAB inhibits the HER pathway, while not disrupting CO_2 reduction. The improved catalytic performance induced by providing surface porosity is ascribed to the hindrance of proton mass transport within the porous network. However, despite the fact that CO_2 saturated 30% (w/w) MEA exhibits many attractive features for using as the reaction medium for electrocatalytic reduction of CO_2, i.e. high carbon dioxide content and high electrical conductivity, prospects for industrial application could be limited since it appears likely that only free CO_2 molecules present at a concentration of around 0.03 M [5f], rather than the major CO_2 containing species $[MEACOO]^-$ can be directly reduced. Further investigations are required to address this issue.

Acknowledgments

L. C. acknowledges Monash University for provision of postgraduate publication award support. The authors also gratefully acknowledge funding provided by Monash University through the Interdisciplinary Research Support Programs and use of the facilities available within the Monash X-ray Platform and the Monash Centre for Electron Spectroscopy

References

[1] D. D. Zhu, J. L. Liu, S. Z. Qiao, *Adv. Mater.* **2016**.

[2] J. F. Brennecke, B. E. Gurkan, *J. Phys. Chem. Lett* **2010**, *1*, 3459-3464.

[3] G. T. Rochelle, *Science* **2009**, *325*, 1652-1654.

[4] G. Puxty, R. Rowland, A. Allport, Q. Yang, M. Bown, R. Burns, M. Maeder, M. Attalla, *Environ. Sci. Technol.* **2009**, *43*, 6427-6433.

[5] aG.-j. Fan, A. G. H. Wee, R. Idem, P. Tontiwachwuthikul, *Ind. Eng. Chem. Res.* **2009**, *48*, 2717-2720; bB. Han, C. Zhou, J. Wu, D. J. Tempel, H. Cheng, *The Journal of Physical Chemistry Letters* **2011**, *2*, 522-526; cV. Souchon, M. de Oliveira Aleixo, O. Delpoux, C. Sagnard, P. Mougin, A. Wender, L. Raynal, *Energy Procedia* **2011**, *4*, 554-561; dG. Richner, G. Puxty, *Ind. Eng. Chem. Res.* **2012**, *51*, 14317-14324; eY. Xiang, M. Yan, Y. S. Choi, D. Young, S. Nesic, *Int. J. Greenh. Gas Control* **2014**, *30*, 125-132; fB. Lv, B. Guo, Z. Zhou, G. Jing, *Environ. Sci. Technol.* **2015**, *49*, 10728-10735; gC. Sun, P. K. Dutta, *Ind. Eng. Chem. Res.* **2016**, *55*, 6276-6283.

[6] M. Ramdin, T. W. de Loos, T. J. H. Vlugt, *Ind. Eng. Chem. Res.* **2012**, *51*, 8149-8177.

[7] aR. Cretu, A. Kellenberger, N. Vaszilcsin, *Int. J. Hydrogen Energy* **2013**, *38*, 11685-11694; bC. C. Văduva, N. Vaszilcsin, A. Kellenberger, *Int. J. Hydrogen Energy* **2012**, *37*, 12089-12096.

[8] D. D. Zhu, J. L. Liu, S. Z. Qiao, *Adv. Mater.* **2016**, *28*, 3423-3452.

[9] aY. Hori, in *Handbook of fuel cells* (Eds.: W. Vielstich, H. A. Gasteiger, A. Lamm, H. Yokokawa), John Wiley & Sons, **2010**, pp. 1-14; bY. Hori, in *Mod. Aspect. Electroc.* (Ed.: C. Vayenas), Springer, New York, **2008**, pp. 89-189.

[10] M. Azuma, K. Hashimoto, M. Hiramoto, M. Watanabe, T. Sakata, *J. Electrochem. Soc.* **1990**, *137*, 1772-1778.

[11] A. S. Hall, Y. Yoon, A. Wuttig, Y. Surendranath, *J. Am. Chem. Soc.* **2015**, *137*, 14834-14837.

[12] S. Sen, D. Liu, G. T. R. Palmore, *ACS Catal.* **2014**, *4*, 3091-3095.

[13] A. Dutta, M. Rahaman, N. C. Luedi, M. Mohos, P. Broekmann, *ACS Catal.* **2016**, *6*, 3804-3814.

[14] aZ. Q. a. J. Weissmuller, *NANO* **2013**, *7*; bJ. R. Hayes, A. M. Hodge, J. Biener, A. V. Hamza, K. Sieradzki, *J. Mater. Res.* **2011**, *21*, 2611-2616.

[15] aK. Chen, X. Zhang, Y. Zhang, D. Y. Lei, H. Li, T. Williams, D. R. MacFarlane, *Advanced Materials Interfaces* **2016**, *3*; bB. J. Plowman, L. A. Jones, S. K. Bhargava, *Chem. Commun.* **2015**, *51*, 4331-4346.

[16] A. I. Bhatt, A. M. Bond, D. R. MacFarlane, J. Zhang, J. L. Scott, C. R. Strauss, P. I. Iotov, S. V. Kalcheva, *Green Chem.* **2006**, *8*, 161-171.

[17] F. Quan, M. Xiong, F. Jia, L. Zhang, *Appl. Surf. Sci.* **2017**, *399*, 48-54.

[18] B. A. Rosen, A. Salehi-Khojin, M. R. Thorson, W. Zhu, D. T. Whipple, P. J. Kenis, R. I. Masel, *Science* **2011**, *334*, 643-644.

[19] B. A. Rosen, J. L. Haan, P. Mukherjee, B. Braunschweig, W. Zhu, A. Salehi-Khojin, D. D. Dlott, R. I. Masel, *J. Phys. Chem. C* **2012**, *116*, 15307-15312.

[20] aJ. Medina-Ramos, R. C. Pupillo, T. P. Keane, J. L. DiMeglio, J. Rosenthal, *J. Am. Chem. Soc.* **2015**, *137*, 5021-5027; bJ. Medina-Ramos, J. L. DiMeglio, J. Rosenthal, *J. Am. Chem. Soc.* **2014**, *136*, 8361-8367; cJ. L. DiMeglio, J. Rosenthal, *J. Am. Chem. Soc.* **2013**, *135*, 8798-8801.

[21] S.-F. Zhao, M. Horne, A. M. Bond, J. Zhang, *J. Phys. Chem. C* **2016**, *120*, 23989-24001.
[22] L. Chen, S. X. Guo, F. Li, C. Bentley, M. Horne, A. M. Bond, J. Zhang, *ChemSusChem* **2016**, *9*, 1271-1278.
[23] J. Zhang, L. Chen, F. Li, C. Bentley, M. Horne, A. Bond, *ChemElectroChem* **2017**, n/a-n/a.
[24] S. Ikeda, T. Takagi, K. Ito, *Bull. Chem. Soc. Jpn.* **1987**, *60*, 2517-2522.
[25] H. C. Shin, J. Dong, M. Liu, *Adv. Mater.* **2003**, *15*, 1610-1614.
[26] A. L. Patterson, *Phys. Rev.* **1939**, *56*, 978-982.
[27] J. Rosen, G. S. Hutchings, Q. Lu, S. Rivera, Y. Zhou, D. G. Vlachos, F. Jiao, *ACS Catal.* **2015**, *5*, 4293-4299.
[28] W. Böttinger, M. Maiwald, H. Hasse, *Fluid Phase Equilib.* **2008**, *263*, 131-143.
[29] A. H. England, A. M. Duffin, C. P. Schwartz, J. S. Uejio, D. Prendergast, R. J. Saykally, *Chem. Phys. Lett.* **2011**, *514*, 187-195.
[30] R. Smith, A. Martell, *Critical Stability Constants, vols. 2–3: Inorganic Complexes/Other Organic Ligands*, Plenum Press, New York, **1976**.
[31] M. Jitaru, D. Lowy, M. Toma, B. Toma, L. Oniciu, *J. Appl. Electrochem.* **1997**, *27*, 875-889.
[32] J. Qiao, Y. Liu, F. Hong, J. Zhang, *Chem. Soc. Rev.* **2014**, *43*, 631-675.
[33] A. Gennaro, A. A. Isse, M. G. Severin, E. Vianello, I. Bhugun, J. M. Savéant, *J. Chem. Soc. Faraday Trans.* **1996**, *92*, 3963-3968.

Supporting Information:

Electrochemical Reduction of Carbon Dioxide in a Monoethanolamine Capture Medium

Lu Chen,[a] Fengwang Li,[a] Ying Zhang, [a] Cameron L. Bentley,[b] Mike Horne,[c]

Alan M. Bond[a] and Jie Zhang*[a]

[a]School of Chemistry and ARC Centre of Excellence for Electromaterials Science, Monash University, Clayton, Vic 3800, Australia

[b]Department of Chemistry, University of Warwick, Coventry, CV4 7AL, U.K.

[c]CSIRO Minerals Resources Flagship, Clayton, Vic 3168, Australia

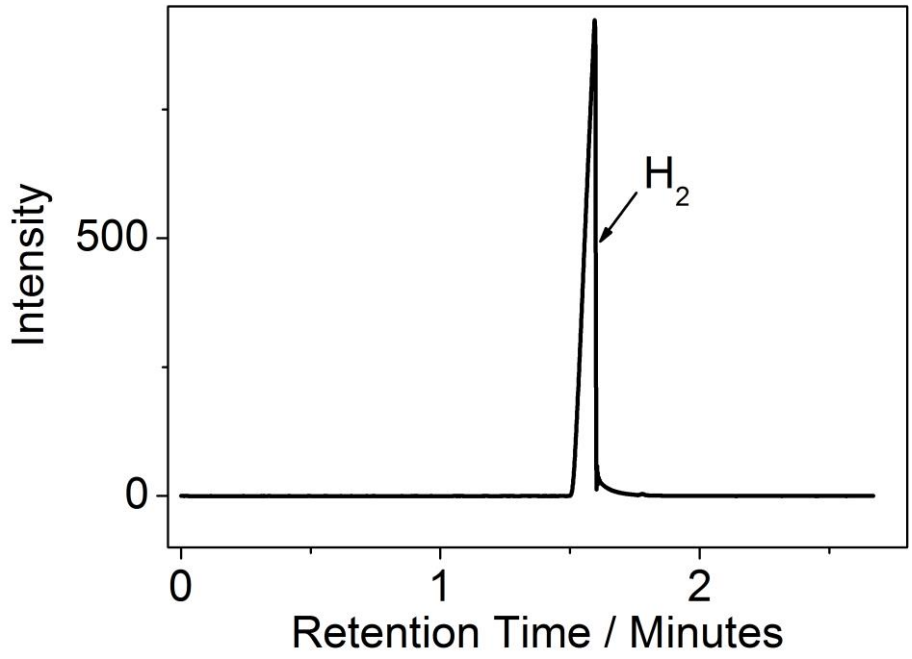

Figure S1: GC identification of the product in the headspace gas after the galvanic reaction of Zn and dimcarb. H_2 with large peak area was detected at retention time of 1.6 minutes. 10 g of Zn powder and 1 mL CO_2 saturated 30% (w/w) MEA aqueous solution were mixed in a 50 ml flask which was degassed with CO_2 and then sealed tightly with a rubber stopper. Magnetic stirring was used to accelerate the reaction rate.

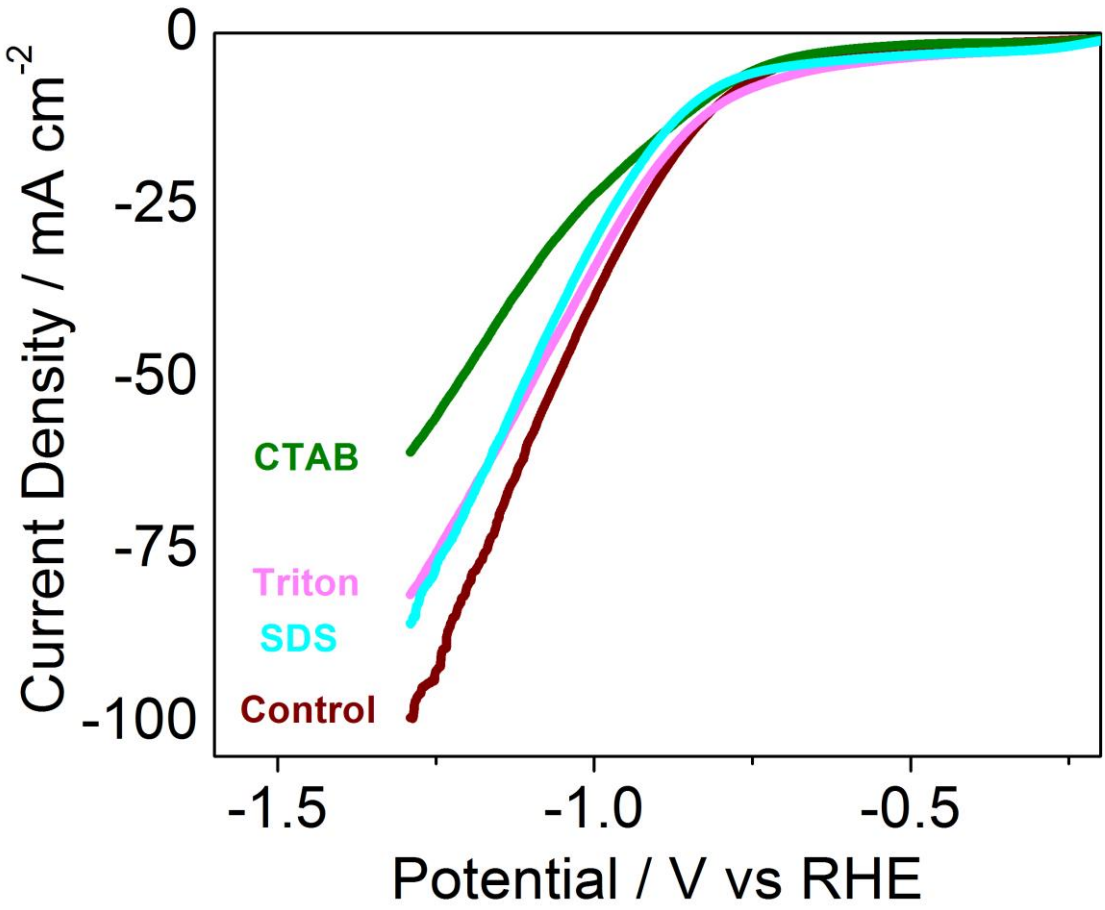

Figure S2: Cyclic voltammograms obtained on a smooth In electrode in CO_2 saturated 30% (w/w) MEA aqueous solution with 0.1% (w/w) CTAB, SDS, Triton X-100 and control experiment (without surfactant).

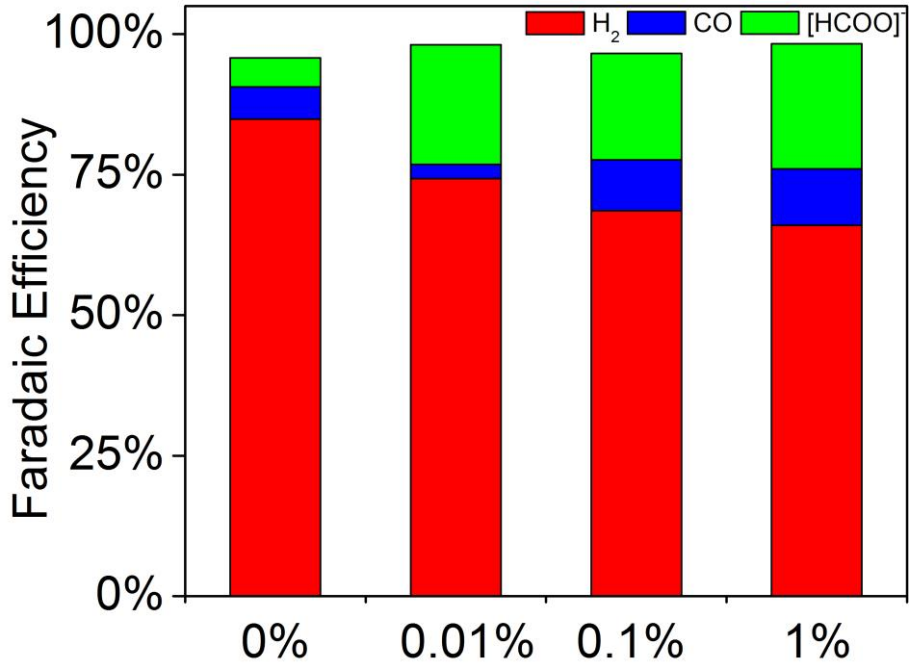

Figure S3: Faradaic efficiencies of the electrolysis products (H_2, CO and $[HCOO]^-$) obtained with a smooth Sn electrode at an applied potential of -0.8 V vs. (RHE) in CO_2 saturated 30% (w/w) MEA aqueous solution with 0%, 0.01%, 0.1% and 1% (w/w)) of CTAB.

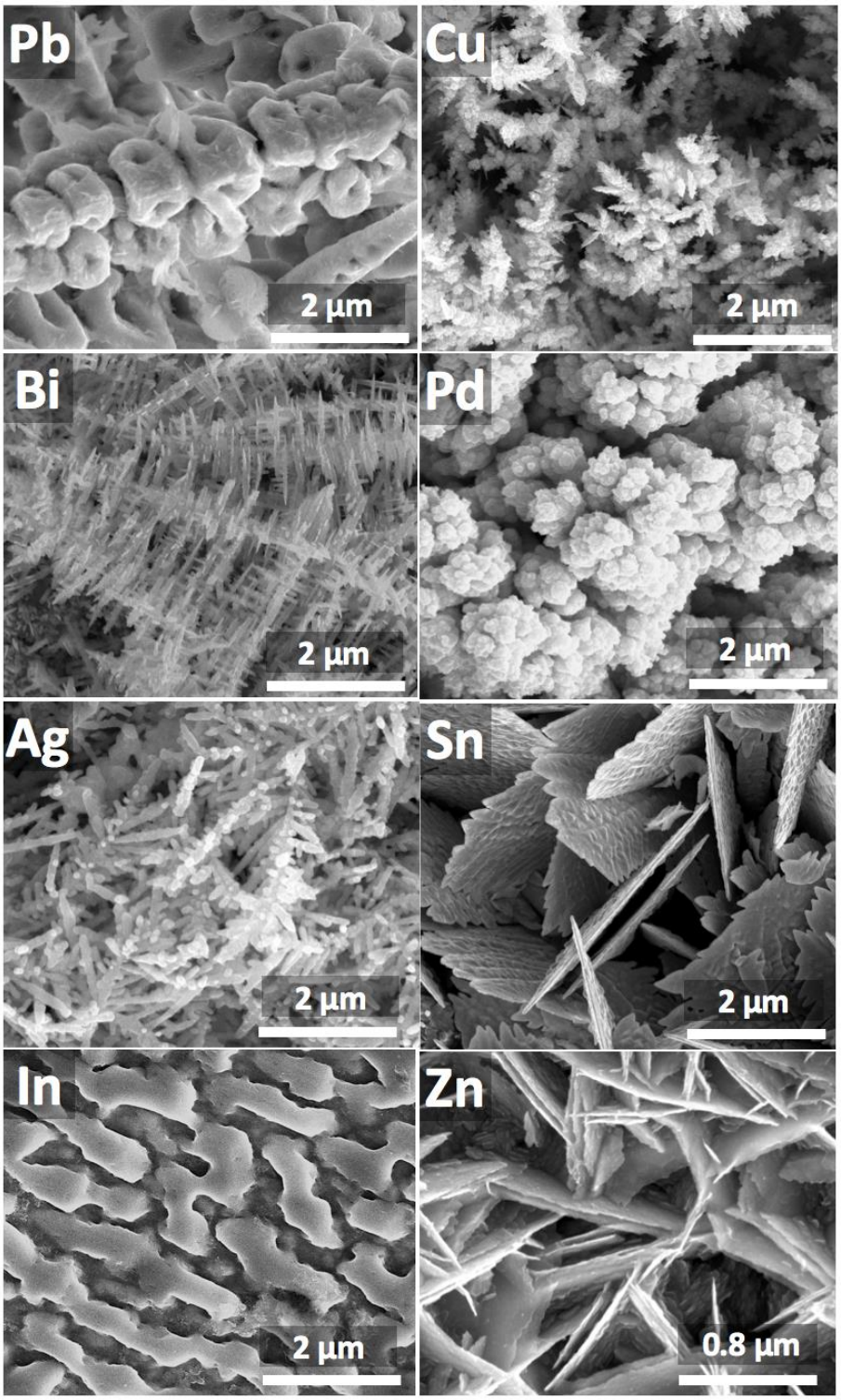

Figure S4: SEM images of the metallic deposits (metals indicated on the respective images) formed by gas bubble templated metal deposition. The deposition parameters are provided in Table S1.

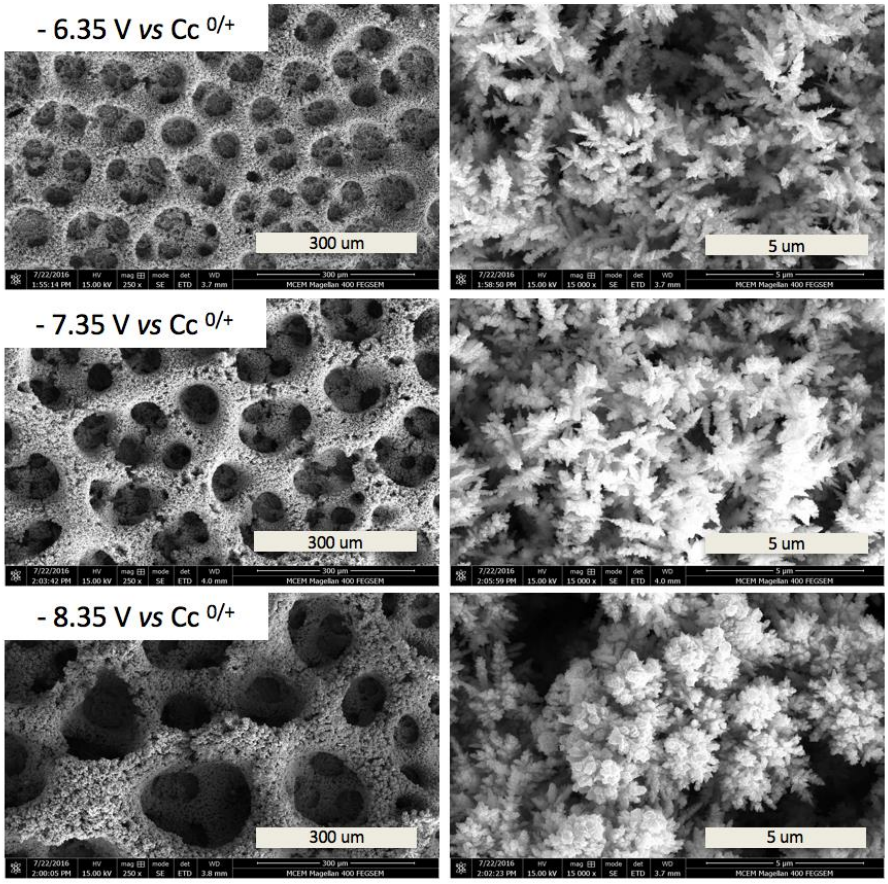

Figure S5: SEM images of Cu electrodeposited on a smooth Cu surface from dimcarb. The deposition was performed by holding the controlled constant potentials at -6.35 V, -7.35 V and -8.35 V vs. ($Cc^{0/+}$) respectively for 30 minutes in dimcarb containing 20 mM CuCl.

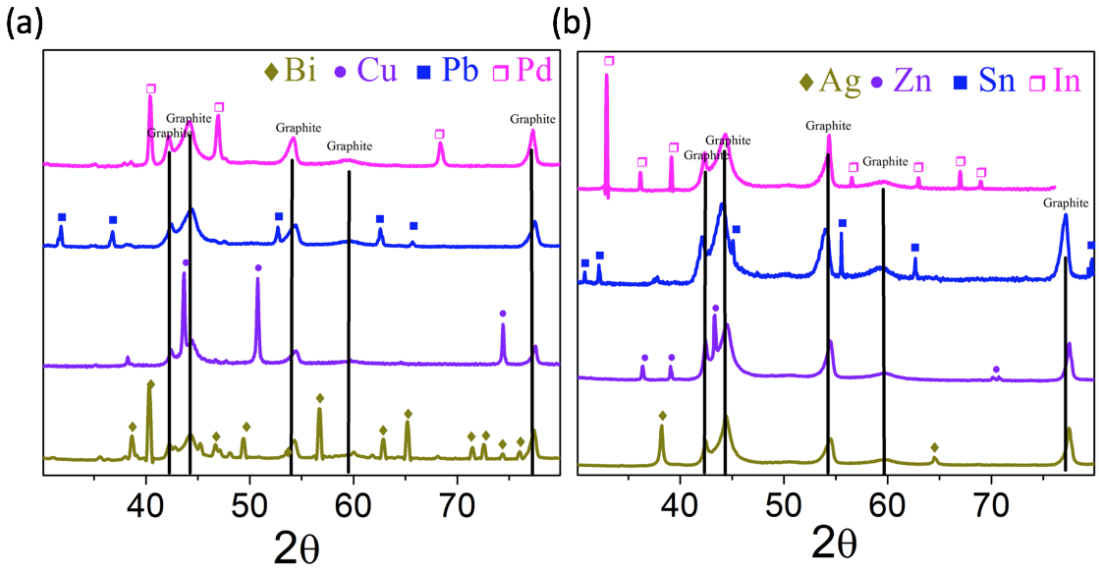

Figure S6: XRD characterization of the 8 metals deposited on graphite plate from dimcarb.

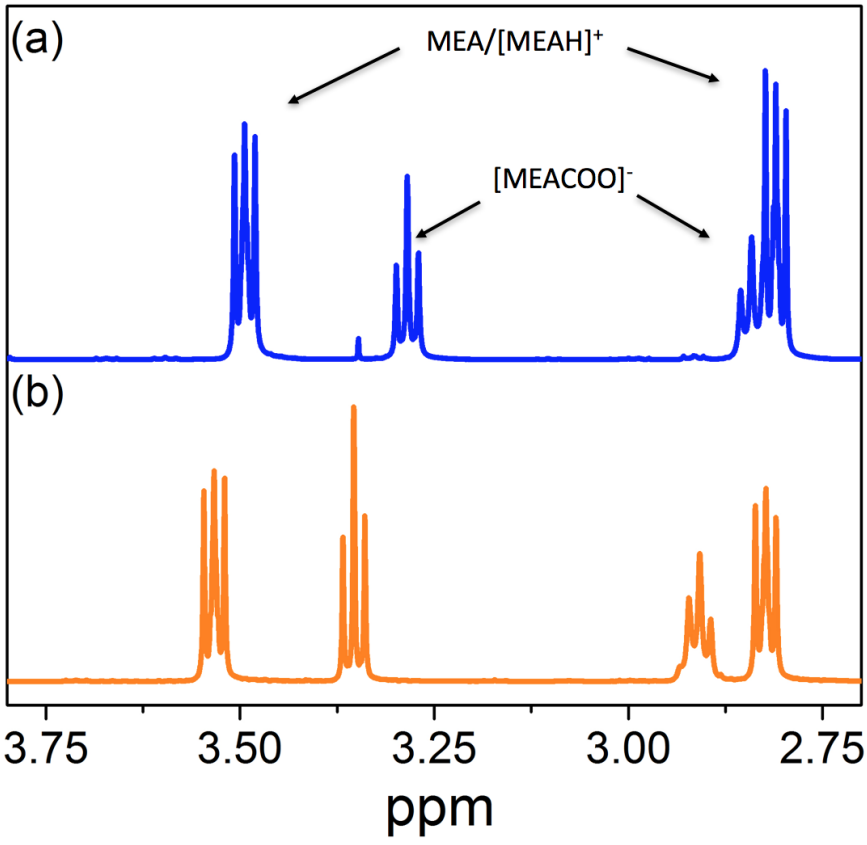

Figure S7: ^{1}H NMR measurements from 30% (w/w) MEA aqueous solution with a mixing molar ratio of CO_2 / MEA of (a) 0.6 and (b) 0.48 in D_2O.

Metal	Deposition Descriptions
Pb	Electrodeposited Pb on smooth Pb in dimcarb containing 40 mM $PbCl_2$ by holding potential at -2.84 V vs. $Cc^{0/+}$ for 1 hour.
Bi	Electrodeposited Bi on smooth Bi in dimcarb containing 20 mM $Bi(NO_3)_3$ by holding potential at -3.34 V vs. $Cc^{0/+}$ for 1 hour.
Sn	Electrodeposited Sn on smooth Sn in dimcarb containing 20 mM $SnSO_4$ by holding potential at -9.34 V vs. $Cc^{0/+}$ for 1 hour.
Cu	Electrodeposited Cu on smooth Cu in dimcarb containing 20 mM CuCl, by holding potential at -7.34 V vs. $Cc^{0/+}$ for 30 minutes.
Pd	Electrodeposited Pd on smooth Pd in dimcarb containing 20 mM $Pd(NO_3)_2$ by holding potential at -7.34 V vs. $Cc^{0/+}$ for 15 minutes.
Ag	Electrodeposited Ag on smooth Ag in dimcarb containing 50 mM $AgNO_3$ by holding potential at -4.34 V vs. $Cc^{0/+}$ for 10 minutes.
In	Electrodeposited In on smooth In in dimcarb containing 10 mM $InCl_3$, by holding potential at -7.34 V vs. $Cc^{0/+}$ for 30 minutes.
Zn	Electrodeposited Zn on smooth Zn in dimcarb containing 100 mM $Zn(Ac)_2$ by holding potential at -9.34 V vs. $Cc^{0/+}$ for 20 minutes.

Table S1: deposition parameters used for fabricating the porous metal surfaces in dimcarb by gas bubble templated metal electrodeposition.

CO_2 loading CO_2/MEA	Metal Electrode	Potential vs. (RHE)	Faradaic Efficiency		
			H_2	CO	$[HCOO]^-$
0.3	In	-0.8	97.7%	a	B
		-1.1	101.0%	a	B
		-1.3	100.0%	a	B
	Ag	-0.8	101.3%	a	B
		-1.1	99.0%	a	B
		-1.3	101.6%	a	B
0.4	In	-0.8	93.4%	a	B
		-1.1	97.2%	a	B
		-1.3	104.9%	a	B
	Ag	-0.8	100.3%	a	B
		-1.1	103.9%	a	B
		-1.3	100.0%	a	B
0.48	In	-0.8	93.9%	0.5%	B
		-1.1	101.8%	0.2%	B
		-1.3	102.1%	a	B
	Ag	-0.8	97.3%	a	B
		-1.1	95.9%	a	B
		-1.3	104.0%	a	B
	a: Below the detection limit. b: Not determined				

Table S2: Bulk electrolysis product distributions (faradaic efficiencies for the generation of H_2 and CO) measured at smooth In and Ag electrodes using three designated applied potentials (-0.8, -1.1 and -1.3 V vs. RHE) in 30% (w/w) MEA aqueous solution with three designated CO_2 loadings (0.3, 0.4, 0.48) in the presence of 0.1% (w/w) CTAB. Since the faradaic efficiency for the generation of H_2 is over 90.0%, the determination of the product in the liquid phase, $[HCOO]^-$, was not performed.